Adsorption of NO on Cu-SAPO-34 and Co-SAPO-34: A Periodic DFT Study

Ellie L. Uzunova,[†,§] Hans Mikosch,*[,‡] and Jürgen Hafner[†]

Faculty of Physics and Center for Computational Material Physics, University of Vienna, Sensengasse 8/12, A-1090 Vienna, Austria, Institute for Chemical Technologies and Analytics, Vienna University of Technology, Getreidemarkt 9/E164/EC, A-1060 Vienna, Austria, and Institute of General and Inorganic Chemistry, Bulgarian Academy of Sciences, Sofia 1113, Bulgaria

Received: September 17, 2007

The location of Cu(I), Cu(II), and Co(II) cations at the extraframework sites of metal cation exchanged SAPO-34 as well as their adsorption properties toward NO are studied by periodic DFT calculations with the PW91 functional. The relative stability of configurations with variable positions of the Si → P substitutions and cation sites was examined; structures with the divalent cation located in proximity to closely spaced negative framework charges were of highest stability. The highest adsorption capacities of the divalent Cu and Co cations were determined for an environment with Si → P substitutions separated in the unit cells, but the interaction between the cation and the more distant negative charges is important for the formation of a stable adsorption complex. The Cu(I)−NO configuration in SAPO-34 is bent, with an angle ∠Cu(I)−N−O of 141.0°. This enables an interaction of the dz^2 state of the cation with both the σ and π^* molecular orbitals. Backdonation to the π^* state leads to a red-shift of the NO stretching frequency by ∼100 cm^{-1}, in good agreement with experiment. For divalent metal cations Cu(II) and Co(II), the highest adsorption energies are related to wider ∠M(II)−N−O angles, shorter M(II)−N bonds, and a slightly weakened N−O bond, indicating a significant electrostatic contribution (ion-dipole interactions) to the bonding and a much less pronounced $d_\pi \rightarrow \pi^*$ back-donation, as reflected by an almost unchanged NO stretching frequency.

Introduction

Nitrogen oxides are harmful to the environment: NO and NO_2 are irritable poisonous gases and though N_2O is used as an anesthetic, when released in the atmosphere it acts as a "greenhouse" gas. The industrial and automotive exhausts are powerful sources of NO_x; therefore, the demand for a more efficient deNO_x process is growing. The selective catalytic reduction of NO by ammonia or hydrocarbons in oxidizing conditions is a rather complex process, and the exact mechanism is far from fully understood. Copper-exchanged zeolites are an alternative to noble metal catalysts for the deNO_x process.[1,2] Cu−MFI is the most extensively studied system because of its high activity in NO decomposition, particularly at high levels of Cu-ion exchange and overexchange (Cu/Al > 0.5). A number of theoretical studies have been devoted to cupric (Cu^{2+}) and cuprous (Cu^+) ions in zeolites and their interaction with NO_x (NO, NO_2, and N_2O), and the role of the local cation environment provided by the zeolite has been elucidated as crucial for the catalytic activity of the transition-metal cation.[3] The modeling of the active sites for NO decomposition has been so far limited mostly to the cluster[3a−c] or embedded-cluster approach.[3d,e] This permits an accurate treatment of the adsorption or reaction complex; however, the zeolite framework is assessed at a lower level of sophistication. Recently, an ab initio DFT calculation of NO adsorption in a fully periodic model of Fe-ferrierite has been presented.[3f]

Among other zeolites and molecular sieves, which have been investigated in NO_x adsorption and disproportionation, the copper-exchanged SAPO-34 had both high catalytic activity and thermal stability.[4] Though SAPOs are structural analogs of zeolites, their physicochemical properties differ considerably from those of aluminosilicate frameworks.[5] It has been argued that the SAPO structure is more covalent because of the inclusion of phosphorus d-orbitals in the bond formation.[6,7] The primary building units of ALPOs consist of PO_4 and AlO_4 tetrahedra. In SAPOs, Si substitutes P at tetrahedral sites and similar to the substitution of Si for Al in zeolites the resulting negative charge is assigned to the framework; a rule of avoidance of Si−O−P linkages has been established as well.[6,8] In Si-rich SAPOs, Si "islands" are formed; thus, substitution of Al by Si is another possible substitution scheme for SAPOs.[8] Transition metals like Cr and Co can be part of the SAPO-34 structure by occupying tetrahedral sites; by cation exchange they take extraframework sites as charge-compensating cations.[6] In the latter case, both redox and Lewis acid−base properties are characteristic for the metal cation centers.

In the present study, the adsorption of NO on Cu^+, Cu^{2+}, and Co^{2+} extraframework cations in SAPO-34 is described by DFT in the generalized gradient approximation (GGA) and using periodic boundary conditions. The relative stability of various Si, Al, and P orderings and how this influences the adsorption capacity of the transition-metal cations was examined. The electronic structure of the adsorption complexes was determined, and the adsorption energies and the vibrational frequency shifts of the NO upon adsorption were calculated.

Structure and Methods

SAPO-34 is a structural analog of the zeolite chabazite (CHA). The framework consists of double six-member rings (D6R), linked by tilted four-member rings such as to form

* Corresponding author. E-mail: hans.mikosch@tuwien.ac.at.
† University of Vienna.
‡ Vienna University of Technology.
§ Bulgarian Academy of Sciences.

10.1021/jp0774903 CCC: $40.75
Published on Web 01/30/2008

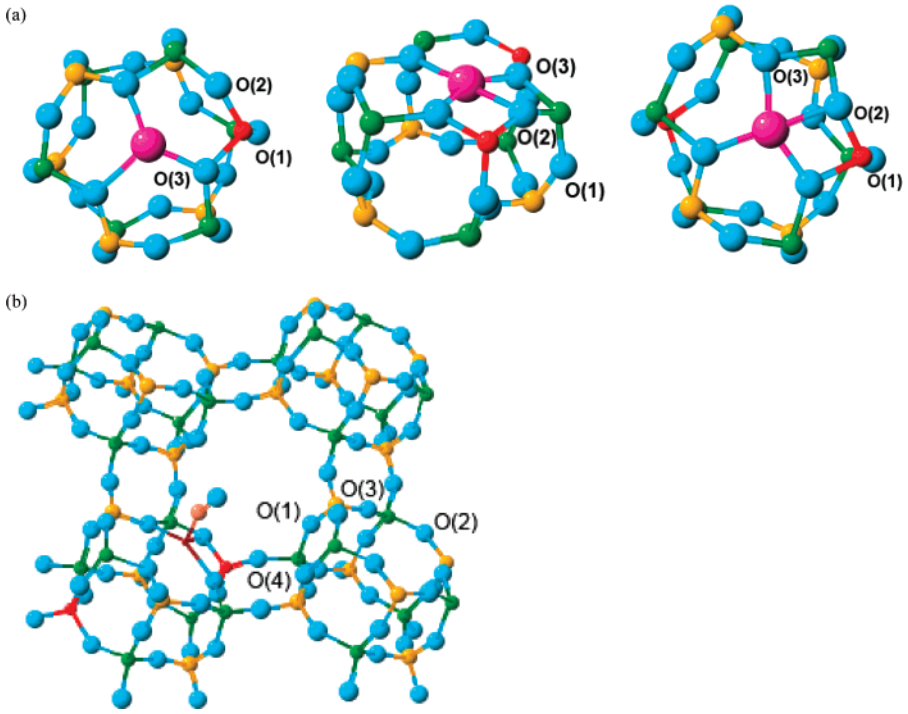

Figure 1. Extraframework of monovalent and divalent cations location in the double six-member rings (D6R) of SAPO-34 with single and double Si → P substitutions. Extraframework cations are denoted by large pink balls, Si atoms are red, Al atoms are green, P atoms are dark yellow, and oxygen atoms are large blue balls. (a) A model consisting of a single unit cell; (b) a larger model with four unit cells and an adsorption complex.

hexagonally stacked layers ABCABC.[9] In the pure aluminophosphate ALPO-34, the Al and P atoms on tetrahedral sites obey strictly alternated ordering and the crystal belongs to the $R\bar{3}$ space group. For SAPO-34 formed as a result of Si → P substitution in ALPO-34, the space group symmetry is lowered to *P*1. The maximum degree of Si → P substitution in SAPO-34 as determined by magic-angle spinning NMR, and element analysis is $x = 1.32$ per unit cell ($H_xSi_xAl_6P_{6-x}O_{24}.nH_2O$).[10,11] Similar to zeolites, the ordering on tetrahedral sites in silicoaluminophosphates cannot be directly evidenced. Assuming a random distribution of the Si atoms, the maximum degree of Si substitution at T sites would require the presence of D6R with twofold Si → P substitutions, while the largest part of D6R would contain a single Si atom. Most of the theoretical and experimental studies of SAPO-34 were performed for a composition with a single Si → P substitution per unit cell.[12,13] The calculations in the present work were performed for the basic rhombohedral unit cell, consisting of 12 T atoms. Monovalent copper extraframework cations were studied in a configuration with a single Si → P substitution in the nearest T_6O_6 ring; the framework charge in D6R with twofold Si → P substitutions was compensated by divalent extraframework cations. It should be noted that applying periodic boundary conditions to a zeolite structure with a relatively small unit cell leads to a highly ordered model of tetrahedral site occupation, which is not realistic. In order to describe specific Si, Al, and P orderings on T sites and also variable Si content and extraframework cation loading, we included models consisting of two and four unit cells explicitly in the calculations. This corresponds to a variation of the Si/Al ratio in the range from 0.0417 to 0.333-(3).

All structural optimizations of SAPO-34, metal-exchanged SAPO-34, and the structures with NO adsorbed were performed with the Vienna ab initio Simulation Package (VASP).[14] The gradient-corrected exchange-correlation functional of Perdew and Wang (PW91)[15] and a plane-wave basis set were used. For the description of the electron−ion interactions, VASP employs the full-potential projector-augmented wave (PAW) method.[16,17] Energy cutoffs of 350 eV were used and the Brillouin-zone sampling was restricted to the Γ point. All calculations have been performed in a spin-polarized mode to account for the spin moments of the paramagnetic NO molecule and of the divalent Cu(II) and Co(II) cations. On adsorption, we always find spin pairing between the adsorbate and extraframework cation to be favored; that is, the Cu(I)−NO complex has spin of $^1/_2$, the Cu-(II)−NO complex is nonmagnetic, and Co(II)−NO has a spin of 1. In the following, we shall not comment in detail on the spin state of the metal-exchanged SAPOs before and after adsorption. The harmonic vibrational frequencies of NO after adsorption were calculated by the finite-difference method.[18] All vibrational frequencies reported in this study are harmonic; an anharmonic correction of ∼26 cm^{-1} was calculated, which applies to the NO stretching frequency in the gas phase as well as for NO adsorbed in zeolites. Molecular properties of the adsorbate molecule (NO) were calculated with VASP and PW91 density functional using a unit cell of 9.0/10.0/11.0 Å (approximately of the size of SAPO-34) and compared to B1LYP calculations with a 6-311+G* basis set using the Gaussian 03 package.[19,20a] The molecular orbital and electrostatic potential maps (MEP) of NO were calculated from the B1LYP density.[20b]

Extraframework Cation Locations and Distribution of Si, Al, and P on Tetrahedral Sites in SAPO-34

Cu(I)-SAPO-34. Monovalent extraframework copper cations compensate a single negative charge in the unit cell of SAPO-34, introduced by a Si → P substitution in a D6R. The cation and the Si atom are placed in proximity; that is, the cation site is located in the T_6O_6 ring with the Si → P substitution ($SiAl_3P_2O_6$), as shown in Figure 1. Calculations have also been performed for a larger supercell containing four unit cells of SAPO-34. This allows us to test the influence of the cation/Al ratio (which is M/Al = 1/6 and M/Al = 1/24 for the small and

TABLE 1: Selected Bond Lengths (Å), Internuclear Distances (Å), and Bond Angles (∠TOT, deg) in Cu(I)-SAPO-34

unit cell	1 Si per single cell	1 Si per 4 UC [a]
Cu−O(3)	1.940; 2.010; 2.354	1.931; 2.003: 2.405
Cu···Si	2.884	2.900
Si−O(3)	1.701	1.703
Al−O(3)	1.757 ÷ 1.837	1.745 ÷ 1.857
P−O(3)	1.538 ÷ 1.567	1.534 ÷ 1.585
∠AlO(3)P	138.2 ÷ 153.8	132.9 ÷ 153.0
∠AlO(4)P	143.8 ÷ 161.4	159.5 ÷ 163.6
∠AlO(3)Si	138.9	131.6
∠AlO(4)Si	142.5	162.3

[a] Si → P substitutions in one D6R only; additional unit cells included in the calculations have the ALPO-34 composition.

large supercells, respectively) and avoids the restrictions imposed by the periodic repetition of a single unit cell. The Si−O(3) bond is elongated, compared to the values typical for zeolites, see Table 1; the value is close to the calculated one for HSAPO-34 at the position of the charge-compensating proton.[12] The Al−O(3) bonds in the $SiAl_3P_2O_6$ ring are elongated even more, and this agrees with experimental data.[10] The Cu(I) cation resides nearly at the center of the $SiAl_3P_2O_6$ ring, slightly closer to the Si atom and forming two shorter and one longer Cu−O(3) bonds. A framework composition with a very low level of Si substitution and Cu(I) loading was considered in order to examine the lattice deformations, introduced by the substitution. The changes in interatomic distances and bond angles in the D6R of SAPO-34 with one Si substitution per four D6R were minor. More significant changes were observed at the unit cell boundary, that is, the stacking of the D6R. The ∠AlO(4)P angles for the low-Si configuration varied in a somewhat narrower range, but the ∠AlO(4)Si angle increased significantly.

Cu(II)-SAPO-34 and Co(II)-SAPO-34. Divalent cations Cu(II) and Co(II) compensate a negative framework charge arising from double Si → P substitution. In the case when the two substitutions occur in the same D6R, two isomeric configurations are possible: one with two Si in the same T_6O_6 ring ($Si_2Al_3PO_6$) and another with one Si per T_6O_6 ring ($SiAl_3P_2O_6$), see Figure 1. In the first configuration a −SiOAlOSi− linkage is formed and the two negative framework charges are separated by only one Al atom. In the second configuration the two Si atoms are separated by a larger distance within the D6R (−SiOAlOPOAlOSi− linkage); however, at high Si content, (e.g., a hypothetical SAPO-34 with double Si → P substitution per D6R and ratio Si/Al = 0.33), a SiOAlOSi linkage appears in the tilted single four-member rings that connect the D6R.

Compared to a monovalent copper cation, the coordination of divalent cations to the framework oxygen atoms changes considerably. The divalent cations approach the nearest negative framework charge center more closely, see Table 2. A local deformation is observed in the T_6O_6 rings where the cations are located; the cations acquire a higher coordination number by binding in addition to an O(2) atom, which is linked to the Si tetrahedral atom. The configuration with maximum separation of the framework negative charges in one D6R, respectively, one Si per T_6O_6 ring, is less stable for both Cu(II) and Co(II) as counter cations, as compared to the configuration with two Si in one T_6O_6 ring, where the negative charges are closely spaced. Assuming Dempsey's rule, which is valid for zeolites and requires maximum separation of the Al atoms (Si is favored at T sites in the sequence T−O−Si−O−Al),[21] one would assume an opposite trend of stability. However, in CHA frameworks configurations with divalent cations (Ca^{2+}) surrounded by closely separated negative framework charges have been proposed as more stable.[22] DFT/B3LYP cluster studies of Ca^{2+} in the D6R of FAU zeolites indicated the highest stability of configurations with two negative framework charges separated by only two T atoms;[23] however, in SAPO-34 the Al, P alternation does not permit exactly the same structure.

The effect of double Si → P substitution per D6R has also been examined at low Si/Al ratios, respectively, at low cation loading. The D6R with Si substitutions was placed in a surrounding of 1 and 3 unit cells without substitution, at the overall ratio Si/Al = 0.0833 ÷ 0.1667, see Tables 2 and 3. The changes in the coordination of metal cation were minor. There is also no substantial difference between the local environment of Cu(II) and Co(II) cations, except that in the configuration with maximum separation of the negative charges Co(II) cations tend to shorten the bond to the fourth oxygen atom from the SAPO-34 framework. When the Si → P substitution is distributed over two D6R with the divalent cation located at a T_6O_6 ring of one D6R as shown in Figure 2, four isomeric configurations emerge. The distance to the second Si substitution varies gradually; see Table 3. A trend of the change in relative stability of the different configurations depending on the distance between the metal extraframework cation and the position of the second Si → P substitution could be established. The relative stability decreases strongly up to a M(II)−Si(2) distance of ca. 7 Å, then remains constant up to ca. 10 Å, followed by a small decrease at longer distances. Thus, we may conclude that the range of the electrostatic field created by the Si centers is limited to these values. In general, the most stable configuration is that with closely spaced negative charges and a divalent cation positioned in the $Si_2Al_3PO_6$ ring. The next stable configuration has both negative charges in one D6R but divided among the two T_6O_6 rings and the divalent cation located in one of them. The configurations with negative charges located in different D6Rs and compensated by a divalent cation in one D6R are all of lower stability, with only a weak dependence on the distance between the metal cation and the more distant Si atom.

NO Adsorption in Cu(I), Cu(II), and Co(II) Exchanged SAPO-34

Adsorbate Molecular Properties. The NO molecule is isoelectronic to O_2^+ and similarly possesses one unpaired electron on an antibonding π^* orbital; the vibrational frequencies of both species are rather close. NO is able to form metal nitrosyls, similar to the metal carbonyls of CO. However, there are differences in the properties of the two molecules, due to the paramagnetic properties of NO and the higher electronegativity of N compared to C. According to ESR spectral studies, 60% of the spin density belongs to the N atom.[24] The NO bond length calculated by the PW91 functional is slightly longer than the experimental value, see Table 4; the vibrational frequency is respectively somewhat underestimated. The PW91 functional overestimates the dissociation energy; however, the enthalpy of formation is determined more accurately:[25]

$$NO \rightleftharpoons {}^1/_2N_2 + {}^1/_2O_2$$

$$\Delta H_f^0 = 90.1 \text{ kJ/mol (PW91); } 87.7 \text{ kJ/mol (B1LYP); } 90.2 \text{ kJ/mol (exp)}$$

The bond length and dissociation energy are determined more accurately by the B1LYP exchange-correlation functional; the dipole momentum, however, is underestimated (0.0781 Db) compared to the experimental value of 0.15872 Db; the

TABLE 2: Selected Bond Lengths (Å) and Internuclear Distances (Å) in M(II)-SAPO-34, (M = Cu, Co) with 2 Si → P Substitution on Different T Sites of a D6R

linkages/ configurations[a]	configuration A: 2 Si in a T_6O_6 ring in D6R		configuration B: 1 Si per each T_6O_6 ring of D6R	
unit cell	1 UC	4 UC	1 UC	4 UC
Cu(II)···Si	2.746; 3.328	2.748; 3.302	2.804; 5.021	2.783; 4.962
Cu−O(3)	1.934; 1.962; 2.272	1.922; 1.956; 2.328	2.003; 2.064; 2.125	1.972; 2.073; 2.147
Cu−O(2)	2.081	2.079	2.123	2.115
Co(II)···Si	2.772; 3.335	2.767; 3.313	2.787; 4.987	2.794; 5.015
Co−O(3)	1.943; 1.989; 2.219	1.931; 1.971; 2.334	1.963; 2.059; 2.120	1.978; 2.081; 2.126
Co−O(2)	2.088	2.096	2.071	2.079

[a] Si → P substitutions in one D6R only; additional unit cells included in the calculations have the ALPO-34 composition.

TABLE 3: Bond Lengths (Å) and Internuclear Distances (Å) in M(II)-SAPO-34, (M = Cu, Co) for Variable Si, P Ordering among 2 D6Rs; Relative Stability ΔE_{st} of the Isomeric Configurations[a]

			−Si−O−Al−O−Si−		−Si−O−Al−O−P−O−Al−O−Si−	
linkages/isomeric configurations[b]	(A): 2 Si per T_6O_6/D6R	(B): 1 Si per T_6O_6/D6R	linkage t_1, Fig. 3	linkage t_3, Fig. 3	linkage t_2, Fig. 3	linkage t_4, Fig. 3
Cu(II)···Si	2.756; 3.322	2.775; 4.973	2.791; 7.028	2.791; 8.442	2.797; 9.899	2.795; 10.925
Cu−O(3)	1.930; 1.969; 2.225	1.973; 2.055; 2.154	1.994; 2.158; 2.221	1.998; 2.159; 2.197	1.973; 2.100; 2.247	1.979; 2.122; 2.227
Cu−O(2)	2.081	2.111	2.175	2.163	2.219	2.203
ΔE_{st}, kJ mol^{-1}	0.00[c]	74.7	131.4	136.9	132.0	122.0
Co(II)···Si	2.784; 3.331	2.788; 5.030	2.770; 6.962	2.765; 8.374	2.773; 9.786	2.772; 10.907
Co−O(3)		1.979; 2.059; 2.140	1.981; 2.070; 2.257	1.978; 2.116; 2.230	1.975; 2.095; 2.251	1.974; 2.100; 2.240
Co−O(2)	2.111	2.076	2.116	2.064	2.087	2.089
ΔE_{st}, kJ mol^{-1}	0.00[c]	83.9	166.3	168.2	166.4	157.3

[a] The supercell contains two unit cells of SAPO34; see Figure 2. [b] Extraframework cation located at one D6R; 1 Si → P substitution per D6R and at different M−Si distances; both D6R included in calculations (two primitive unit cells). [c] Reference zero energy for each isomeric configuration.

TABLE 4: Calculated Bond Length (R), Dissociation Energy (D), and Harmonic and Vibrational Frequency υ for the NO Molecule

method	R_{N-O}, Å	D, kJ mol^{-1}	υ, cm^{-1} [a]
PW91	1.169	729.43	1876
B1LYP/ 6-311+G*	1.146	612.68	1998
exp 25	1.1508	631.62 ± 0.18	1904

[a] Anharmonic correction: −26 cm^{-1}.

harmonic vibrational frequency is overestimated, and the correction for anharmonicity does not improve the result too much. A number of experimental[26] and theoretical[27−29] studies have considered the binding of NO to transition-metal cations in the gas phase. The binding mechanism to the transition-metal cation is generally understood as synergic, as the σ-dative bond formed with the lone pair orbital at the N atom is reinforced by π-backdonation from the π-type d orbitals (d_π) of the transition metal to the singly occupied π^* orbital of NO.[31] According to this scheme, as the extent of backdonation increases, the M−N bond becomes stronger, while the N−O bond becomes weaker. The molecular electrostatic potential (MEP) map of NO indicates that the σ lone pair orbital at the N atom forms together with the partly occupied π^* orbital a broad region of high nucleophilicity around the N atom, see Figure 3. Similarly, the lone pair orbitals at the O atom also give rise to nucleophilic properties at the oxygen atom; however, the potential at the N atom is much stronger. The lone pair orbitals of both N and O are, however, of considerably lower energy as compared to the π^* orbital. The MEP maps also indicate that if NO is coordinated to the TM (transition metal) cation via the oxygen atom then the structure will always be bent, while binding of NO via the N atom will result in either the linear or bent configuration. In a linear configuration, a strong electrostatic component may contribute to the bonding, but for symmetry reasons the molecular σ orbital can interact only with the dz^2 atomic orbital of the cation, and the π^* orbitals only with the d_π orbitals. In a bent configuration, other interactions (such as, e.g., between a dz^2 orbital and the π^* orbitals) may also play a significant role. Previous theoretical studies have shown that the binding via the N atom is strongly preferred.[26−28]

NO Adsorption on Cu(I) and Cu(II) Extraframework Cations in SAPO-34. Our results for the NO adsorption complex at mono- and divalent copper cations in SAPO-34 with different Si → P substitutions in one or two D6R (see Figure 4) are summarized in Tables 5 and 6. The results for monovalent Cu(I) compensating a single Si → P substitution and for divalent Cu(II) as a charge-compensating cation for two Si → P substitutions located in the same D6R are listed in Table 5 (the two possible configurations for divalent cations are shown in Figure 1). Calculations have been performed for supercells containing one or four unit cells of SAPO-34 (i.e., one or four D6R) and hence metal-cation ratios of M/Al = $^1/_6$ and M/Al = $^1/_{24}$, respectively. In general, we find only a modest influence of the size of the supercell on the adsorption properties, but in the case of a divalent Cu cation located closely to both Si sites (linkage −Si−O(2)−Al−O(3)−Si−) we find that the restricted flexibility of the SAPO framework in a supercell cell consisting of only a single unit cell may hinder a full relaxation of the adsorbate/framework complex and result in a significantly reduced adsorption energy, although the geometry and the NO stretching frequency are almost unchanged. The results for Cu(II) and Co(II) as charge-compensating cations for Si substitu-

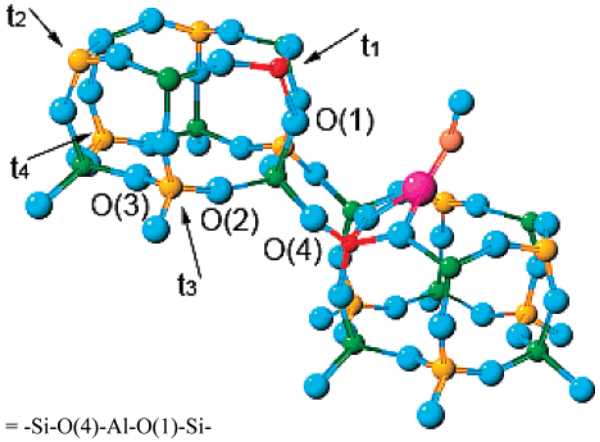

t_1 = -Si-O(4)-Al-O(1)-Si-
t_2 = -Si-O(4)-Al-O(2)-P-O(3)-Al-O(2)-Si-
t_3 = -Si-O(4)-Al-O(2)-Si-
t_4 = -Si-O(4)-Al-O(2)-P-O(3)-Al-O(1)-Si-

Figure 2. Extraframework cation location of monovalent and divalent cations in D6R of SAPO-34 with one Si per D6R and variable Si, P ordering among two unit cells. One Si → P substitution is always in a tetrahedral site next to an O(4) oxygen atom (lower D6R), and the metal cation is located in the same T_6O_6 ring. The second Si atom is placed on different tetrahedral sites in the second D6R (sites t1−t4). The linkages between the two Si atoms are denoted.

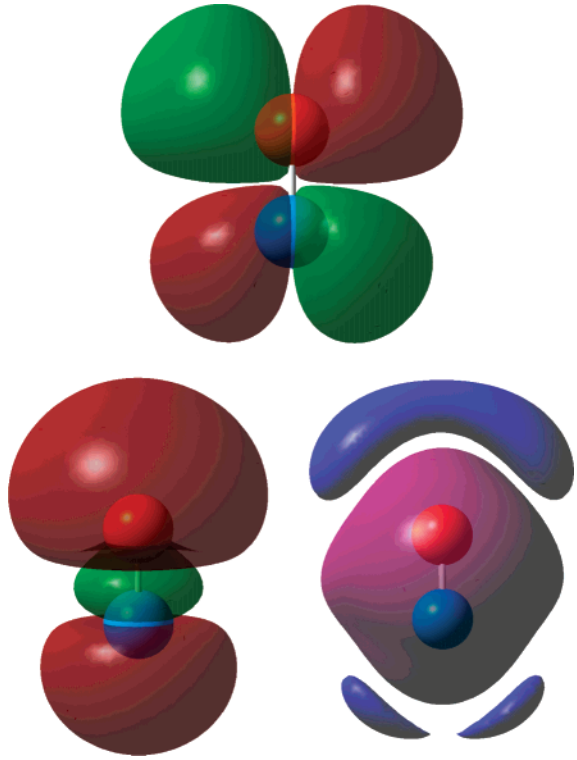

Figure 3. π^* orbital; the σ-lone-pair orbital; and the molecular electrostatic potential (MEP) map (au) of NO: nitrogen atoms are orange, oxygen atoms are light-blue, red and green colors represent the positive and negative parts of molecular orbitals, and red and blue colors represent positive and negative regions of MEP maps.

tions in two different D6Rs are summarized in Table 6; the configurations t_1 to t_4 are defined in Figure 2. The cation is always located close to one Si site (distance M−Si ≈ 2.8 Å); the distance to the second Si site varies in the range 7−11 Å, see Table 3. In addition, we have considered the two configurations with both Si in the same D6R and short (configuration A, with a short Si−Si distance; −Si−O−Al−O−Si− linkage and configuration B with a longer Si−Si distance; linkage −Si−O−Al−O−P−O−Al−O−Si−) and long Si−Si distance, see

A. Link sequence : -Si-O(2)-Al-O(3)-Si-

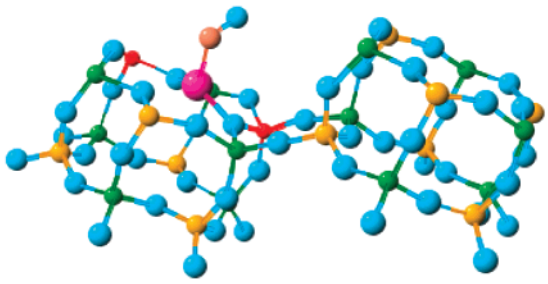

B. Link sequence : -Si-O(2)-Al-O(3)-P-O(2)-Al-O(1)-Si-

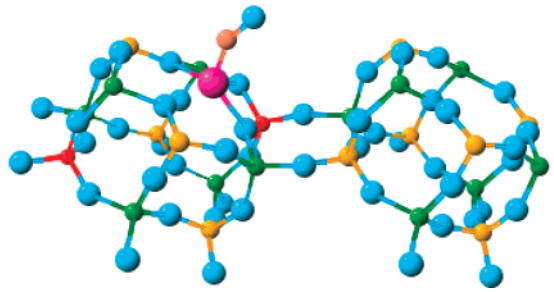

Figure 4. Adsorption complex in structures with variable positions of two Si atoms in the D6R of SAPO-34. A model with two D6R included in calculations.

Figure 4. For the NO adsorption at a Cu(I) cation, the angle ∠Cu(I)−N−O is 141.0° and it is even smaller for ∠Cu(II)−N−O: 129.0 ÷ 137.0°. The tilted configuration shows that the π^* states of NO play an important role in the Cu−NO bonding. In Cu(I), the metal cation d-orbitals are fully occupied and thus unable to accept electrons from the NO; however, back-donation from the d orbitals to the partly filled π^* orbital of NO takes place, as evidenced by the elongated N−O bond and the red-shifted vibrational frequency. Calculations of the interaction between Cu^+ and NO in the gas phase have indicated that the vacant Cu 4s orbital becomes populated, and a one-electron bonding between copper and nitrogen is formed.[28] This results in a shortened N−O bond length, while the Cu−N bond was relatively long. However, the coordination of the metal cations to a zeolite or, as in our case, silicoaluminophosphate framework, changes the properties of the adsorption centers. The monovalent copper cations become able to back-donate electrons and this leads to a stronger Cu−N bond, and a weaker N−O bond. The Cu(I) cation remains coordinated to only two oxygen framework atoms after adsorption and it moves closer to the Si atom, respectively, the two oxygens, O(2) and O(3), bonded to Si. In the NO stretching frequency, this is reflected by a red-shift of ∼116 cm^{-1}, in good agreement with a measured shift of ∼99 cm^{-1}.[30] For NO adsorption on Cu(I), we find only a negligible dependence on the size of the supercell in the calculations.

The adsorption of NO on Cu(II) produces a slightly lower adsorption energy, a shortened N−O bond, and a vibrational frequency that is almost unchanged compared to gas-phase NO. A slight blue shift is calculated for configurations with closely spaced Si atoms, (configurations t_1 and A). This indicates a donation of electron density from NO to the vacant d-orbital of Cu(II), while the effect of back-donation is less-pronounced. Upon adsorption, Cu(II) cations also move in the direction of the Si → P substituted tetrahedral sites. In the configuration with closely spaced Si atoms, the coordination number of the Cu(II) cation is lowered from 4 to 2 and the cation approaches the region of the two Si centers. The blue-shifted vibrational

TABLE 5: Selected Bond Lengths (Å), Bond Angles (deg), Adsorption Energies, and Linear Vibrational Frequency v of the NO Molecule Adsorbed on Isolated Extraframework Cations Cu(I), Cu(II), and Co(II) in SAPO-34 and Frequency Shift Δv Relative to the Calculated Gas-Phase Frequency[a]

cations/ configurations	$R_{M-O(z)}$, Å [b]	R_{M-NO}, Å	R_{N-O}, Å	∠M−NO	E_{ads}, kJ mol^{-1}	v,[c] cm^{-1}	Δv, cm^{-1}
Cu^{+}							
	1.987; 2.041 (1.999; 2.034)	1.763 (1.762)[d]	1.187 (1.187)	141.0 (141.2)	124.6 (129.1)	1760 (1763)	−116
Cu^{2+}							
A	1.910; 1.938; 2.415; 2.759 (1.934; 1.959; 2.241; 2.784)	1.797 (1.804)	1.151 (1.150)	129.2 (128.8)	118.9 (53.0)	1889 (1888)	+13
B	1.940; 2.083; 2.194; 2.811	1.818	1.155	130.7	109.4	1855	−21
Co^{2+}							
A	1.954; 2.037; 2.069; 2.720 (1.961; 2.044; 2.087; 2.522)	1.679 (1.682)	1.160 (1.160)	169.8 (169.3)	195.2 (192.8)	1924 (1918)	+48
B	1.982; 2.080; 2.130; 2.491	1.686	1.163	158.7	182.0	1884	+8

[a] The supercell consists of four unit cells; the metal cation per Al ratio is M/Al = 0.0417 (one metal cation per four D6R). [b] Internuclear distances between metal cations and the nearest oxygens from the SAPO-34 framework: three O(3) and the one O(2) connected to Si. [c] Experimental vibrational frequencies from ref 29: Cu(I)-SAPO-34/NO: 1806 cm^{-1} (Δv = −98 cm^{-1}); Cu(II)-SAPO-34/NO: 1901 cm^{-1} (Δv = −3 cm^{-1}); Co(II)-SAPO-34/NO: 1900 and 1814 cm^{-1} (Δv = −4 and −90 cm^{-1}). [d] Numbers in parentheses give results for one cation/D6R and single unit cell.

TABLE 6: Selected Bond Lengths (Å), Bond Angles (deg), Adsorption Energies, and Linear Vibrational Frequency v of the NO Molecule Adsorbed on a M(II) Cation in Cu(II)-SAPO-34 and Co(II)-SAPO-34 with Variable Si, P Ordering[a]

cations/ configurations	$R_{M-O(z)}$, Å [b]	R_{M-NO}, Å	R_{N-O}, Å	∠M−NO	E_{ads}, kJ mol^{-1}	v,[c] cm^{-1}	Δv, cm^{-1}
Cu^{2+}							
t_1	1.950; 1.975; >2.9	1.725	1.163	161.0	142.0	1883	7
t_3	1.951; 1.978; >2.9	1.726	1.164	160.9	137.5	1875	no shift
t_2	1.955; 1.976; >2.9	1.726	1.163	159.9	128.7	1875	no shift
t_4	1.955; 1.983; >2.9	1.727	1.164	160.3	130.1	1873	no shift
A	1.913; 1.942; 2.347; 2.759	1.794	1.151	130.5	102.7	1892	+16
B	1.957; 2.208; 2.237; 2.537	1.782	1.157	136.5	89.1	1861	−15
Co^{2+}							
t_1	2.006; 2.023; 2.226; >2.7	1.670	1.169	157.0	223.5	1854	−22
t_3	2.010; 2.017; 2.232; >2.7	1.665	1.168	164.7	218.2	1870	−6
t_2	2.002; 2.043; 2.182; >2.7	1.672	1.169	156.0	218.9	1848	−28
t_4	2.003; 2.037; 2.200; >2.7	1.662	1.168	165.7	217.9	1869	−7
A	1.954; 2.035; 2.091; 2.595	1.679	1.161	167.3	184.7	1874	no shift
B	1.990; 2.073; 2.103; 2.498	1.684	1.163	158.5	196.6	1883	+6

[a] In configurations t1−t4 Si atoms are placed in two different D6R; see Figure 2. Configurations A and B have both Si atoms in the same D6R; see Figure 4. [b] Internuclear distances between metal cations and the nearest oxygen atoms from the SAPO-34 framework O(3) and the O(2) connected to Si. [c] Experimental vibrational frequencies: see Table 5.

frequency of NO is related to more-pronounced Lewis acid properties of the cation center in this case; the effect of 4sdσ hybridization,[31] which was proposed for the interaction NO with bare transition-metal cations, might play an important role for the NO binding to both Cu(I) and Cu(II) cations in SAPO-34. In the configuration with largely separated Si atoms within a D6R, the Cu(II) remains nearly centered at the T_6O_6 ring ($SiAl_3P_2O_6$) and coordinated to the three O(3) framework atoms. The NO vibration frequency is in this case slightly red-shifted.

Divalent copper cations have higher NO adsorption capacity in configurations where the Si → P substitutions are in different D6Rs, that is, where the second negative framework charge is more distant, see Figure 2. The angle ∠Cu(II)−N−O increases considerably, the N−O bond length also increases, and the N−O vibrational frequency becomes slightly red-shifted, see Table 6. The highest adsorption energies are observed for configurations with more closely spaced Si atoms (see Figure 4); however, the distance between substitutions in neighboring D6R is always longer than that for substitutions in the same D6R. An electrostatic ion-dipole contribution to the bonding can be

TABLE 7: Selected Bond Lengths (Å), Bond Angles (deg), Adsorption Energies, and Linear Vibrational Frequency υ of Two NO Molecules Adsorbed on Single Isolated Co(II) Extraframework Cations in SAPO-34 (1 Metal Cation per 4 UC; Respectively Ratio M/Al = 0.0417)

configurations	$R_{Co-O(z)}$, Å [a]	R_{Co-NO}, Å	$R_{N-O,}$ Å	∠Co−NO, deg	∠NCoN, deg	E_{ads}, kJ mol^{-1}	υ,[b] cm^{-1}
A	2.028; 2.045	1.666; 1.670	1.161; 1.164	157.7; 158.7	105.4	268.1	1888; 1857
B	2.032; 2.056	1.660; 1.668	1.164; 1.165	156.7; 158.9	104.8	357.5	1886; 1857

[a] Internuclear distances between metal cations and the nearest oxygens from the SAPO-34 framework O(3) and the O(2) connected to Si. [b] Experimental vibrational frequencies: see Table 5.

deduced for these adsorption complexes together with significant effect of π-back-donation. The coordination number of Cu(II) in configurations with negative framework charges separated in different D6R is lowered to two upon adsorption; the cation moves in the direction to the closely positioned negative framework charge and remains coordinated to the two oxygens bonded to this Si atom. For configuration A (where both Si atoms reside on the same T_6O_6 ring), we note a surprisingly strong dependence of the adsorption energy on the size of the supercell. If only one unit cell is considered in the calculations, then the relaxation of the adsorption complex (lowering of the Cu(II) coordination number to framework oxygen atoms) is restricted because of the limitations arising from a periodic repetition of the framework structure over short distances. The Cu(II) cation is forced to remain rather close to three framework oxygens, resulting in a dramatically reduced adsorption capacity; see Table 5. No similar effect arises if the Si substitution sites are distributed over different T_6O_6 rings.

NO Adsorption on Co(II) Extraframework Cations in SAPO-34. The Co−N bond in the adsorption complex of NO with Co(II) cations is shorter, compared to the adsorption complexes with Cu(I) and Cu(II), and the adsorption energies are significantly higher. Because Co(II) possesses vacant d-orbitals, both σ- and π-dative bonds can be formed. Indeed, the geometries of all adsorption complexes approach a linear structure, although a weak bending is observed. The NO vibration frequency is strongly blue-shifted in the configuration with closely spaced negative framework charges; however, this occurs only at lowest metal cation loadings, that is, an isolated adsorption center among three "neutral" unit cells; see Table 5. Minor blue-shift of the frequency is also detected for a configuration with a larger distance between Si atoms, but within the same D6R; the angle ∠Co(II)−N−O decreases for both Si/Al = 0.0833 and 0.1667, that is, for two and four D6Rs included in calculations. The Co(II) cation remains nearly four-coordinated to the framework oxygen atoms; however, it also moves in direction to the Si → P substitutions and one of the Co−O(3) bonds becomes significantly elongated.

In configurations where the Si → P substitutions are in two neighboring D6Rs (see Table 6), a different structure of the adsorption complexes is observed. The Co(II) cations approach the nearest Si atom and form two shorter bonds with the oxygen atoms bonded to Si and one longer bond to the next nearest O(3) atom; the coordination number to the framework is thus reduced to 3. The NO vibration frequency experiences a very small red shift, which indicates a certain π back-donation from the d_π orbitals of the metal cation to the π^* orbital of NO. The predicted small red shift is in good agreement with the experimental observation (υ_{NO} = 1900 cm^{-1}). A large adsorption energy together with a bond length and stretching frequency that are almost unchanged with respect to the gas phase is a remarkable result. This shows that in contrast to NO adsorption on extended metallic surfaces[32] σ-donation dominates over π-backdonation. Though a stable tendency of ∠Co(II)−N−O bending could not be traced, the NO frequency red shift can be related to a more strongly bent adsorption complex also for Co(II) exchanged SAPO-34; the adsorption energy increases as well.

Multiple NO Adsorption on Cu(I) and Co(II) Extraframework Cations in SAPO-34. Although direct measurements of adsorption energy for metal-exchanged SAPO-34 are not available, our calculated adsorption energies agree with measurements on Cu(I)- and Cu(II)-exchanged zeolites.[33] IR studies on Cu(I)- and Co(II)-exchanged SAPO-34 have indicated the formation of di-nitrosyls; they are also considered important as intermediates in the deNOx process. Recent ab initio and IR studies of NO adsorption in Fe-ferrierite demonstrate a capacity to adsorb two or more NO molecules per extraframework cation.[3f] We have found the formation of dinitrosyls only in the Co(II) exchanged SAPO-34, see Table 7. All attempts to adsorb two NO molecules on Cu(I) or Cu(II) in SAPO-34 were unsuccessful, and the second NO molecule drifted away from the cation in the SAPO cavity. Thus, our suggestion is that the vibrational frequency assigned to dinitrosyls of Cu(I) in SAPO-34 [30] should be modified; according to our results, bands of lower frequency are rather due to mononytrosyls of Cu(II) in a specific local environment of the extraframework cation, for example, in a configuration with two tetrahedral Si atoms placed at a maximum distance within one D6R and at low Si/Al ratio [see Table 5 (configuration B) and Figure 1b]. Co(II) adsorbs two NO molecules readily, and the structure of the adsorption complex for each NO molecule is similar to the one determined for mono-adsorption; that is, a similar bonding scheme can be assumed (see Table 7). However the coordination number of Co(II) to the framework oxygen is reduced to two. In the case of dinitrosyl formation, the adsorption capacity of the configuration with largely separated framework charges within the D6R is significantly higher. The vibrational spectrum of the dinitrosyl complex consists of a symmetric and an asymmetric NO stretching mode. The frequency of the symmetric mode is almost unchanged compared to the Co(II) mononitrosyl; the asymmetric mode is lower by ∼30 cm^{-1}. Experimental data suggest a somewhat larger splitting.

Conclusions

The adsorption properties of transition-metal cations Cu(I), Cu(II), and Co(II) in SAPO-34 strongly depend on their coordination to the framework. The NO adsorption complexes of Cu(I) and Cu(II) are bent; this also holds for Co(II); however, the angle ∠Co(II)−N−O is in general broader. This agrees with previous theoretical studies for bare cations, which found linear adsorption complexes for the 3d elements Cr−Ni and bent adsorption complexes for Cu;[27] the bonding mechanism, however, differs considerably in a SAPO-34 environment. The electron donor−acceptor properties of the metal cations are strongly modified by the framework. For bent adsorption complexes, σ-donation and π-backdonation are no longer strictly

distinct processes because the interaction between the dz^2 orbital of the cation and the π^* orbital of the adsorbate are no longer symmetry-forbidden; the metal−nitrogen bond formation is also favored by 4sdσ hybridization. The cations reduce their coordination number to framework oxygen atoms upon NO adsorption and move in direction to the nearest negative framework charge; Cu(I) remains coordinated to two oxygen atoms, Cu(II) and Co(II) strongly increase their adsorption capacity in a local environment with a distant second negative framework charge; the angle ∠Cu(II)−N−O is broadened, and in this case Cu(II) also remains only twofold coordinated to framework oxygen atoms after adsorption. The Co(II) cations have the highest adsorption capacity; they have a capacity to bind at least two molecules.

Acknowledgment. This work has been supported by the Austrian Science Funds under project no. P17020-NO2 and by the Institut Francais du Petrole within the cooperation with the Universität Wien. We gratefully acknowledge CPU time at the Computer Center, Technical University Vienna, where most of the calculations were performed. ELU gratefully acknowledges the hospitality of the University of Vienna and the Center for Computational Materials Physics.

References and Notes

(1) Richter-Addo, G. B.; Legzdins, P. *Metal Nitrosyls*; Oxford University Press: New York, 1992.

(2) (a) Kuroda, Y.; Iwamoto, M. *Top. Catal.* **2004**, *28*, 111. (b) Iwamoto, M.; Yokoo, S.; Sakai, K.; Kagawa, S. *J. Chem. Soc., Faraday Trans.* **1981**, *77*, 1629. (c) Iwamoto, M. *Zeolites and Related Microporous Materials: State of the Art 1994, 10th International Zeolite Conference Garmisch-Partenkirchen*; Weitcamp, J., Karge, H. G., Pfeifer, H., Hölderich, W., Eds.; Elsevier: Amsterdam, 1994; p 1395. (d) Li, Y.; Hall, W. K. *J. Phys. Chem.* **1990**, *94*, 6145. (e) Beutel, T.; Sárkány, J.; Lei, G.-D.; Yan, J.; Sachtler, W. M. H. *J. Phys. Chem.* **1996**, *100*, 845.

(3) (a) Trout, B. L.; Chakraborty, A. K.; Bell, A. T. *J. Phys. Chem.* **1996**, *100*, 17582. (b) Rice, M. J.; Chakraborty, A. K.; Bell, A. T. *J. Phys. Chem. B* **2000**, *104*, 9987. (c) Schneider, W. F.; Hass, K. C.; Ramprasad, R.; Adams, J. B. *J. Phys. Chem. B* **1998**, *102*, 3692. (d) Santiago, L. R.; Sierka, M.; Branchadell, V.; Sodupe, M.; Sauer, J. *J. Am. Chem. Soc.* **1998**, *120*, 1545. (e) Davidová, M.; Nachtigallová, D.; Nachtigall, P.; Sauer, J. *J. Phys. Chem. B* **2004**, *108*, 13674. (f) Benco, L.; Bucko, T.; Grybos, R.; Hafner, J.; Sobalik, Z.; Dedecek, J.; Hrusak, J *J. Phys. Chem. C* **2007**, *11*, 586.

(4) Ishihara, T.; Kagawa, M.; Hadama, F.; Takita, Y. *Zeolites and Related Microporous Materials: State of the Art 1994, 10th International Zeolite Conference Garmisch-Partenkirchen*; Weitcamp, J., Karge, H. G., Pfeifer, H., Hölderich, W., Eds.; Elsevier: Amsterdam, 1994; p 1493.

(5) (a) Wilson, S. T.; Lok, B. M.; Messina, C. A; Cannan, T. R.; Flanigen, E. M. *J. Am. Chem. Soc.* **1982**, *104*, 1146. (b) Lok, B. M.; Messina, C. A.; Patton, R. L.; Gajek, R. T.; Cannan, T. R.; Flanigen, E. M. *J. Am. Chem. Soc.* **1984**, *106*, 6092.

(6) Pastore, H. O.; Coluccia, S.; Marchese, L. *Annu. Rev. Mater. Res.* **2005**, *35*, 351.

(7) Corà, F.; Catlow, CRA. *J. Phys. Chem. B* **2001**, *105*, 10278.

(8) Sastre, G.; Lewis, D. W.; Catlow, C. R. A. *J. Phys. Chem. B* **1997**, *101*, 5249.

(9) Baerlocher, Ch.; Meier, W. M.; Olson D. H. *Atlas of Zeolite Framework Types*, 5th revised edition; Elsevier: Amsterdam, 2001.

(10) (a) Smith, L. J.; Cheetham, A. K.; Morris, R. E.; Marchese, L.; Thomas, J. M.; Wright, P. A. *Science* **1996**, *271*, 799. (b) Smith, L. J.; Cheetham, A. K.; Marchese, L.; Thomas, J. M.; Wright, P. A.; Chen, J.; Gianotti, E. *Catal. Lett.* **1996**, *41*, 13.

(11) (a) Marchese, L.; Chen, J.; Wright, P. A.; Thomas, J. M. *J. Phys. Chem.* **1993**, *97*, 8109. (b) Anderson, M. W.; Sulikowski, B.; Barrie, P. J.; Klinowski, J. *J. Phys. Chem.* **1990**, *94*, 2130.

(12) Jeanvoine, Y.; Angyan, J.; Kresse, G.; Hafner, J. *J. Phys. Chem. B* **1998**, *102*, 5573.

(13) Anderson, M. W.; Sulikowski, B.; Barrie, P. J.; Klinowski, J. *J. Phys. Chem.* **1990**, *94*, 2130.

(14) (a) Kresse, G.; Hafner, J. *Phys. Rev. B* **1993**, *48*, 13115. (b) Kresse, G.; Hafner, J. *Phys. Rev. B* **1994**, *49*, 14251. (c) Kresse, G.; Furthmüller, *J. Comput. Mater. Sci.* **1996**, *6*, 15. (d) Kresse, G.; Furthmüller, J. *Phys. Rev. B* **1996**, *54*, 11169.

(15) Perdew, J. P.; Chevary, J. A.; Vosko, S. H.; Jackson, K. A.; Pederson, M. R.; Singh, D. J.; Fiolhais, C. *Phys. Rev. B* **1992**, *46*, 6671.

(16) Blöchl, P. E. *Phys. Rev. B* **1994**, *50*, 17953.

(17) Kresse, G.; Joubert, D. *Phys. Rev. B* **1999**, *59*, 1758.

(18) Kresse, G.; Furthmüller, J.; Hafner, J. *Europhys. Lett.* **1995**, *32*, 729.

(19) (a) Lee, C.; Yang, W.; Parr, R. G. *Phys. Rev.* **1988**, *B37*, 785−789. (b) Miehlich, B.; Savin, A.; Stoll, H.; Preuss, H. *Chem. Phys. Lett.* **1989**, *157*, 200. (c) Becke, A. D. *J. Chem. Phys.* **1993**, *98*, 5648. (d) Becke, A. D. *J. Chem. Phys.* **1996**, *104*, 1040.

(20) (a) Frisch, M. J.; Trucks, G. W.; Schlegel, H. B.; Scuseria, G. E.; Robb, M. A.; Cheeseman, J. R.; Montgomery, J. A., Jr.; Vreven, T.; Kudin, K. N.; Burant, J. C.; Millam, J. M.; Iyengar, S. S.; Tomasi, J.; Barone, V.; Mennucci, B.; Cossi, M.; Scalmani, G.; Rega, N.; Petersson, G. A.; Nakatsuji, H.; Hada, M.; Ehara, M.; Toyota, K.; Fukuda, R.; Hasegawa, J.; Ishida, M.; Nakajima, T.; Honda, Y.; Kitao, O.; Nakai, H.; Klene, M.; Li, X.; Knox, J. E.; Hratchian, H. P.; Cross, J. B.; Bakken, V.; Adamo, C.; Jaramillo, J.; Gomperts, R.; Stratmann, R. E.; Yazyev, O.; Austin, A. J.; Cammi, R.; Pomelli, C.; Ochterski, J. W.; Ayala, P. Y.; Morokuma, K.; Voth, G. A.; Salvador, P.; Dannenberg, J. J.; Zakrzewski, V. G.; Dapprich, S.; Daniels, A. D.; Strain, M. C.; Farkas, O.; Malick, D. K.; Rabuck, A. D.; Raghavachari, K.; Foresman, J. B.; Ortiz, J. V.; Cui, Q.; Baboul, A. G.; Clifford, S.; Cioslowski, J.; Stefanov, B. B.; Liu, G.; Liashenko, A.; Piskorz, P.; Komaromi, I.; Martin, R. L.; Fox, D. J.; Keith, T.; Al-Laham, M. A.; Peng, C. Y.; Nanayakkara, A.; Challacombe, M.; Gill, P. M. W.; Johnson, B.; Chen, W.; Wong, M. W.; Gonzalez, C.; Pople, J. A. *Gaussian 03*, revision C.02; Gaussian, Inc.: Wallingford, CT, 2004. (b) Dennington, R., II; Keith, T.; Millam, J.; Eppinnett, K.; Hovell, W. L.; Gilliland, R. *GaussView*, Version 3.09; Semichem, Inc.: Shawnee Mission, KS, 2003.

(21) Dempsey, E. *J. Phys. Chem.* **1969**, *73*, 3660.

(22) (a) Takaishi, T. *J. Phys. Chem.* **1995**, *99*, 10982. (b) Takaishi, T.; Kato, M.; Itabashi, K. *Zeolites* **1995**, *15*, 21.

(23) Uzunova, E.; Mikosch, H. *J. Phys. Chem. B* **2004**, *108*, 6981.

(24) Enemark, J. H.; Feltham, R. D. *Coord. Chem. Rev.* **1974**, *13*, 339.

(25) *Handbook of Chemistry and Physics*, 85th ed.; CRC Press: Boca Raton, FL, 2004−2005.

(26) (a) Zhou, M.; Andrews. L. *J. Phys. Chem. A* **2000**, *104*, 2618. (b) Zhou, M.; Andrews. L. *J. Phys. Chem. A* **2000**, *104*, 3915.

(27) Thomas, J.; Bauschlicher, C. W., Jr.; Hall, M. B. *J. Phys. Chem. A* **1997**, *101*, 8530.

(28) Koszinowski, K.; Schröder, D.; Schwarz, H.; Holthausen, M. C.; Sauer, J.; Koizumi, H.; Armentrout, P. B. *Inorg. Chem.* **2002**, *41*, 5882.

(29) (a) Cassady, J. C.; Freiser, B. S. *J. Am. Chem. Soc.* **1985**, *107*, 1566. (b) Khan, F. A.; Steele, D. L.; Armentrout, P. B. *J. Phys. Chem.* **1995**, *99*, 7819.

(30) (a) Akolekar, D. B.; Bhargava, S. K.; Foger, K. *J. Chem. Soc., Faraday Trans.* **1998**, *94*, 155. (b) Akolekar, D. B.; Bhargava, S. K. *Appl. Catal., A* **2001**, *207*, 355.

(31) Bauschlicher, C. W., Jr.; Langhoff, S. R.; Partridge, H. *J. Chem. Phys.* **1991**, *94*, 2068.

(32) Gajdos, M.; Hafner, J.; Eichler, A. *J. Phys. Condens. Matter* **2006**, *18*, 13.

(33) Gervasini, A.; Picciau, C.; Auroux, A. *Microporous Mesoporous Mater.* **2000**, *35*−*36*, 457.